

Modeling musician diffraction and absorption for artificially excited clarinet directivity measurements

Samuel David Bellows and Timothy Ward Leishman

Citation: *Proc. Mtgs. Acoust.* **46**, 035002 (2022); doi: 10.1121/2.0001586

View online: <https://doi.org/10.1121/2.0001586>

View Table of Contents: <https://asa.scitation.org/toc/pma/46/1>

Published by the [Acoustical Society of America](#)



Why Publish in POMA?

Watch Now 



182nd Meeting of the Acoustical Society of America

Denver, Colorado

23-27 May 2022

*Musical Acoustics: Paper 3aMU1

Modeling musician diffraction and absorption for artificially excited clarinet directivity measurements

Samuel David Bellows and Timothy Ward Leishman

*Department of Physics and Astronomy, Brigham Young University, Provo, UT, 84602;
samuel.bellows11@gmail.com; tim_leishman@byu.edu*

Directivity measurements of musical instruments have many applications in musical, audio, and architectural acoustics. Typical measurement methods include artificially excited instruments and instruments played by live musicians. While recent advances in directivity measurement techniques enable higher resolutions for played instruments, the results are still limited in bandwidth and repeatability compared with directivity results from artificially excited instruments. However, artificially excited instruments typically neglect musician diffraction and absorption. This work compares possible approaches for representing musician diffraction in artificially excited clarinet measurements to improve their directivity results for room simulations or auralizations.

POMA Student Paper Competition Winner

1. INTRODUCTION

The directivities of musical instruments have many applications in audio, architectural, and musical acoustics, allowing researchers and practitioners to improve microphone placements, room acoustical designs, auralizations, and sound source modeling. Previous works related to musical instrument directivity measurements have employed natural and artificial instrument excitation in anechoic environments (i.e., with and without musicians). Nevertheless, while the directivities of isolated instruments have merits, the intrinsic impacts of diffraction and absorption by musicians are critical for more realistic practical results.¹ Unfortunately, these musician effects often receive little attention or are simply neglected. This paper explores the effects and how one might provide correction for isolated instrument directivities, beginning with the clarinet as an example.

The primary advantage of artificial excitation is that it allows quasi-repeatable sound production, which is especially advantageous for multiple-capture measurements that scan instrument radiation in many directions, such as for high-resolution measurements² or acoustical holography.³ Despite artificial excitation's utility in these and other areas, it requires specially constructed playing apparatuses. Because the excitation methods influence how instruments produce and radiate sound, researchers should exercise great care to ensure that their techniques produce results similar to natural excitation for realistic results. However researchers often develop widely varying apparatus designs and methods, even for select instrument types. For example, violin directivity measurements have employed reciprocity techniques,⁴ Lorentz-force-based techniques,⁵ and bowing machines.⁶ Artificial excitation additionally requires researchers to design and construct new playing apparatuses for each instrument or instrument family. Difficulties introduced by these apparatuses can result in extensive measurement times to consider full instrument working ranges. Consequently, many studies have limited their directivities to only a few notes and their associated partials.

In contrast, natural instrument excitation ensures normal playing under realistic conditions and facilitates measurements of full instrument working ranges without technical difficulties. However, its lack of repeatability between multiple captures has limited spatial sampling resolutions with fixed numbers of microphone positions, e.g., 13, 32, or 64, in circular or spherical arrays.⁷⁻⁹ Various normalization schemes have compensated for instrument playing variability, enabling multiple-capture measurements to be more effective.^{1, 10-12} More recently, a frequency-response-function (FRF)-based approach has allowed the measurement of sixteen musical instruments at 2,522 positions over a sphere, conforming to the AES loudspeaker directivity sampling standard.^{13,14} Nonetheless, even FRFs are limited in frequency range due to high signal-to-noise ratio requirements and they cannot compensate for musician movements.

Another advantage of natural excitation is that it allows a streamlined approach to measuring multiple instruments using the same measurement setup. Thus, this method dominates the literature in terms of the number of instruments considered in each study, e.g., 3 in Ref. 7, 4 in Ref. 10, 16 in Ref. 13, and 41 in Ref. 8. Finally, because natural excitations typically employ musicians in normal playing positions, they are best suited for many applications such as room acoustical design or auralizations. Indeed, these applications motivated many naturally excited musical instrument directivity studies.^{7, 8, 10, 11, 13, 15}

Despite recent directivity measurement trends, many directional data from isolated instrument studies still exist. In addition, the repeatability of artificial excitation measurements remains a significant advantage over natural excitation measurements. Consequently, researchers and practitioners would benefit from better understanding how musicians alter the directivities of isolated instruments for various applications. This work accordingly explores the effects of musician diffraction and absorption on musical instrument directivities. It proposes distinct approaches allowing experimentalists to perform measurements with artificial excitation while still accounting (to an extent) for the acoustical effects of a musician's body. The following sections consider several theoretical, experimental, and modeling concepts related to musician diffraction and absorption. They discuss and compare measured directivities results from an artificially excited clarinet, with and without proposed corrections, to those of a naturally played clarinet.

2. BASIC CONCEPTS OF MUSICIAN DIFFRACTION AND ABSORPTION

Although enough time and resources might overcome many of the mentioned limitations of artificial excitation, musician diffraction and absorption still play an essential role in musical instrument directivities and should not be ignored for many applications. To better appreciate the effects that diffraction can have on source directivity, first consider the simple case of a point source radiating into free space in comparison to the source radiating near a rigid spherical scatterer.¹⁶ Without the scattering body, the far-field directivity is omnidirectional, but with the scatterer, the directional features change dramatically at higher frequencies. Figure 1 illustrates this for various ka , with k being the wavenumber and a being the radius of the sphere. The distance between the point source and the sphere's center is $1.5a$. For large wavelengths ($ka \ll 1$), the scattering body has minimal effect on the directivity. However, as the wavelength becomes sizable to the scattering body, deviations from omnidirectionality become visible. Undulating levels indicate constructive and destructive interference regions due to varying path lengths. Behind the sphere, a diffraction spot appears, which is also apparent for speech and other directivities.¹⁷

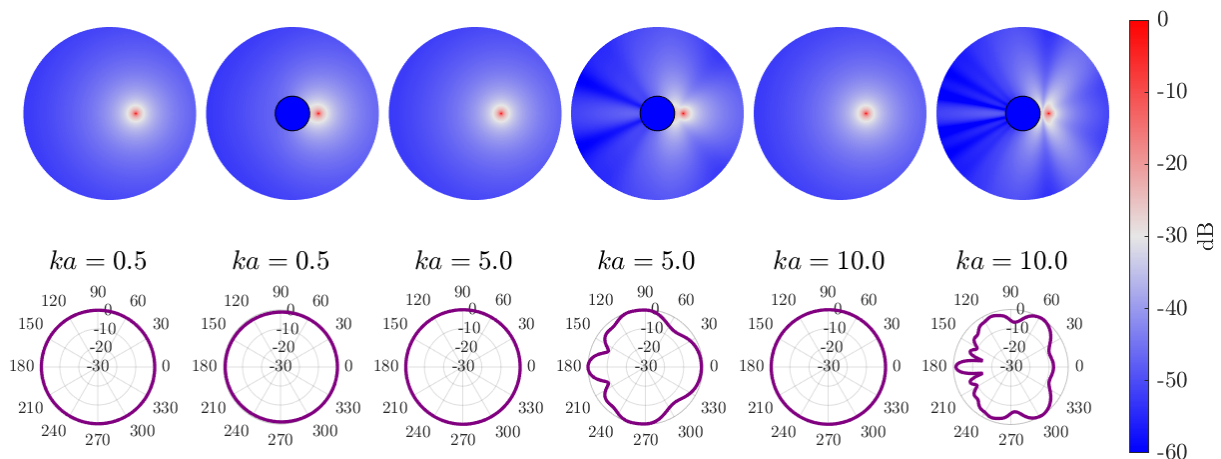


Figure 1: Scattering effects on the directivity of a point source without and with the presence of a rigid spherical scatterer for selected ka , following the developments in Ref. 16. The plot conditions alternate from left to right. Top row: Color-mapped pressure magnitudes on a plane through the point source and the sphere's center. Bottom row: Polar plots of the far-field directivity patterns.

Comparisons of measured directivity patterns often reveal similar diffraction effects from one source to another, despite differences in sound-generation mechanisms. Figure 2 shows this effect for the violin and speech in the 400, 500, and 800 Hz 1/3rd-octave bands, with both color and radius showing relative levels on a 40 dB scale. While each source produces and radiates sound differently, the directional characteristics at these frequencies are similar due to the diffraction of the human body. At higher frequencies, the similarities decrease, in part due to the position of the source relative to the body; nonetheless, the plots show that diffraction plays an important role in measured source directivities.

3. MODELING DIFFRACTION AND ABSORPTION WITH ARRAY SHADING

Because musician diffraction and absorption significantly affect source directivity, several applications require their inclusion. A simple means of fulfilling this need for artificially excited instrument directivity measurements would be to include a dressed mannequin in the measurement setup. This approach has been

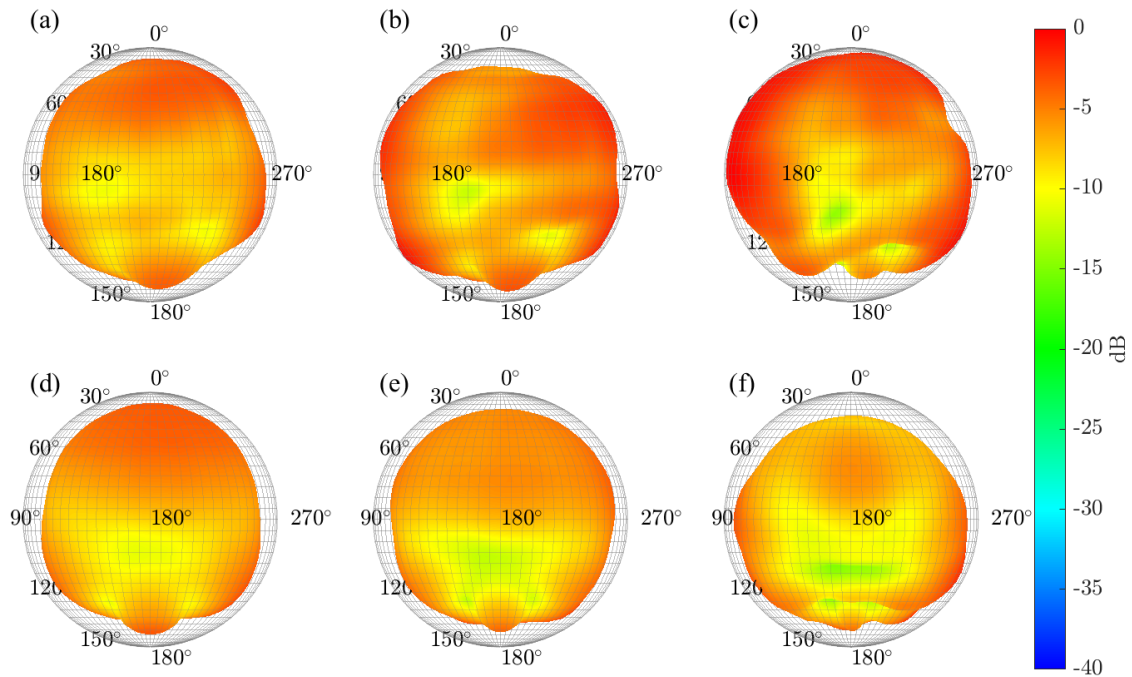


Figure 2: Directivity balloons for the violin (a)-(c) and human speech (d)-(f) in the 400 Hz [(a), (d)], 500 Hz [(b), (e)], and 800 Hz [(c), (f)] 1/3rd-octave bands. The vantage point is from behind the violinist and talker. All balloons are based on degree $N = 18$ spherical harmonic expansions.

commonly used for speech measurements^{17–19} but not musical instrument measurements. However, in some situations, such as when the size of the measurement room limits the maximum measurement array size, a mannequin may not be feasible.

One straightforward alternative is to shade the isolated instrument’s measured directivity pattern to simulate musician diffraction and absorption. That is, based on a measured directivity function D , the shaded directivity function D_s becomes

$$D_s(\theta, \phi, f) = W(\theta, \phi, f)D(\theta, \phi, f), \quad (1)$$

where $W(\theta, \phi, f)$ is the weight or shading function. Such shading is commonly used with arrays to control beam pattern performance, but this section highlights two possible shading functions to mimic diffraction and absorption effects. Results for measured data appear in Sec. 5.

Some researchers have measured frequency-dependent attenuation behind musicians,^{1,20} but have not developed formulations to apply the attenuation to isolated instruments measurements. One possibility to accomplish this is to use a generalized cardioid pattern in both angular coordinates as a shading function:

$$W_L(\theta, \phi, f) = \frac{\alpha(f) + \sin \theta \cos \phi}{\alpha(f) + 1} \quad (2)$$

where

$$\alpha(f) = \frac{10^{-L(f)/20} + 1}{10^{-L(f)/20} - 1} \quad (3)$$

and $L(f)$ is the desired attenuation in dB. Figure 3 shows the normalized shading balloons for varying L .

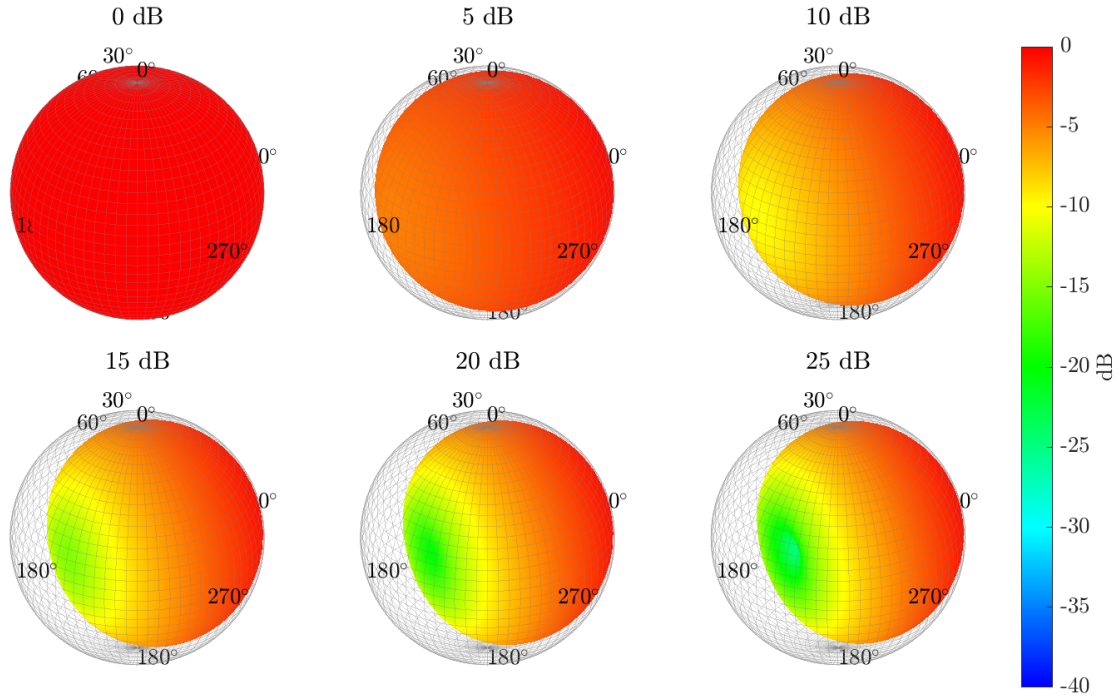


Figure 3: Normalized shading function W_L for various levels of attenuation L .

If the attenuation is unknown, a theoretical model can estimate the parameter $\alpha(f)$. For this work, the scattering of radiation from a point source a distance a_0 from the center of nearby rigid sphere of radius a provided a basic understanding of the attenuation. The difference between the maximum pressure and the pressure directly behind the sphere provided the attenuation estimate. To mitigate the effects of strongly fluctuating attenuation values due to strong diffraction lobes such as those seen directly behind the sphere in Figs. 1 and 5, an $N = 4$ spherical harmonic expansion of the pressure smoothed these features. Figure 4 shows the resultant curves for the parameter $\alpha(f)$. The curves reveal that at low frequencies, the spherical body produces only minimal attenuation on its opposing side. At higher frequencies, the attenuation becomes much more significant.

While Eq. (2) provides a simple shading function if the attenuation behind the musician is known or estimated, it does not include wave phenomena such as diffraction lobes or spots. An alternative shading function that includes these effect follows from the radiation of sound from a point source on the sphere.²¹ The unnormalized weights are

$$W_s(\theta, \phi) = \sum_{n=0}^{\infty} \sum_{m=-n}^n \frac{h_n^{(2)}(ka)}{h_n^{(2)'}(ka)} Y_n^m(\theta, \phi) [Y_n^m(\theta_0, \phi_0)]^*, \quad (4)$$

where $h_n^{(2)}$ are the spherical Hankel functions of the second kind of order n (for outward-going waves with $e^{i\omega t}$ time dependence), Y_n^m are the normalized spherical harmonics of degree n and order m , $*$ denotes complex conjugation, and (θ_0, ϕ_0) is the angular position of the point source on the sphere of radius a . For this shading function, the radius of the sphere controls the frequency-dependent nature of the attenuation. Thus, to apply the function, the parameter a could be estimated from the dimensions of a scattering body or through modeling. In this work, minimizing differences between measured directivities and W_s at low frequencies determined the effective body radius. The authors first determined the directivity factor function¹⁶ of a given note's fundamental. The effective scatterer radius then followed by finding the value of a

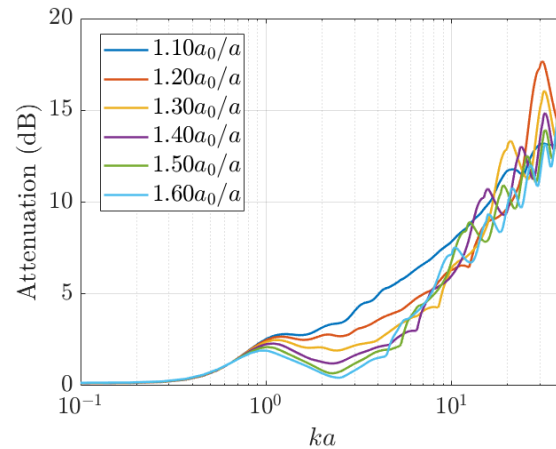


Figure 4: Values of attenuation based on scattering from a rigid sphere of radius a due to a point source placed at position $r = a_0$.

that minimized the deviation between the measured directivity factor function and W_s . Figure 5 shows the shading functions for selected ka values. Diffraction spots appear in several of the directivity balloons.

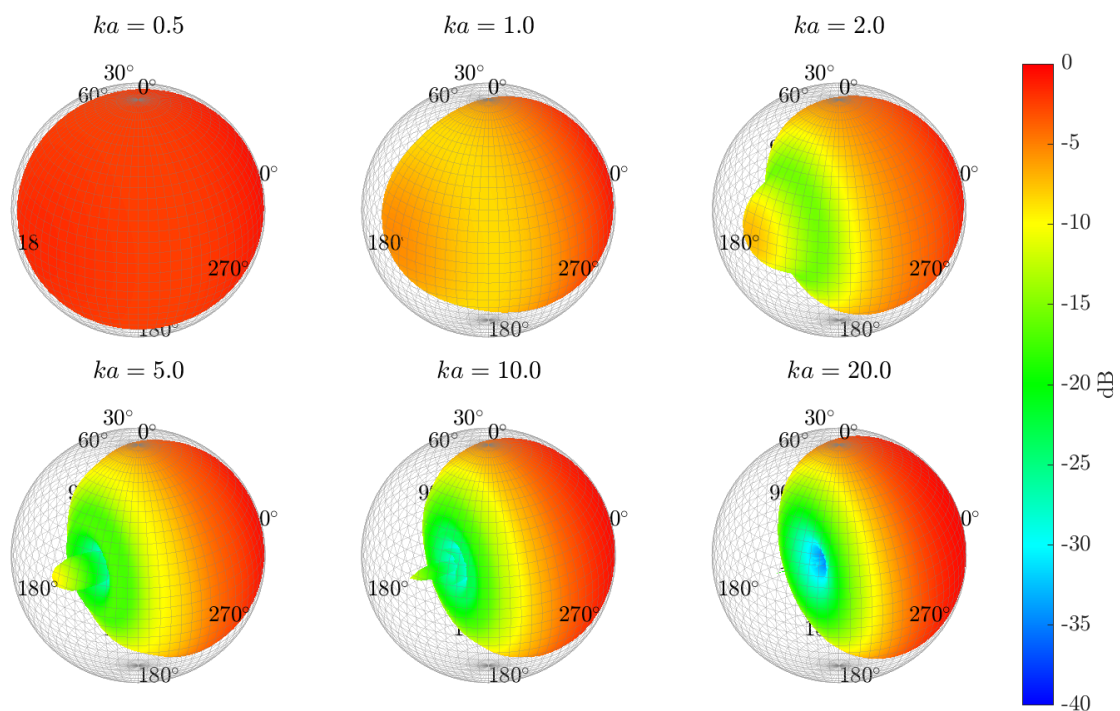


Figure 5: Normalized balloons of the shading function W_s for a point source on a sphere at $(\theta_0, \phi_0) = (\pi/2, 0)$ and various ka values. Diffraction spots and generally increasing attenuation appear behind the sphere with increasing frequency.

4. DIRECTIVITY MEASUREMENTS

To study the effects of a musician's body on measurement results, the authors assessed a B \flat clarinet's directivity using three different methods. Figure 6 shows each measurement setup: (1) the isolated instrument (oriented upside-down) excited artificially using a blower, (2) the instrument and blowing apparatus attached to a seated mannequin with the blowing apparatus replacing the head, and (3) the instrument played by a musician. The semi-circular scanning array included 36 12.7 mm (0.5 in.) microphones positioned with 5° polar angular spacing. Array rotations in 5° azimuthal steps enabled a full-spherical measurement conforming to the AES sampling standard¹⁴ with the omission of the south pole position. Data processing with FRFs provided normalization for each capture, which was essential for the naturally played instrument.^{13,17} The measurement radius for the artificial blower configurations, including with the mannequin, was $a = 0.98$ m, while for the live musician, it was $a = 1.17$ m. Post-processing rotations and acoustical holography produced far-field directivities of all sampled pressures for equitable comparisons.^{21,22}

5. RESULTS

A. DIFFRACTION EFFECTS

The measurements revealed that musician diffraction and absorption effects are significant even at lower frequencies. Figure 7 shows far-field projected directivities for the clarinet E4 fundamental (328 Hz). While the isolated instrument pattern in Fig. 7(a) appears to be roughly omnidirectional, both the artificially excited instrument with the mannequin and the played instrument have stronger radiation regions in front of the instrument and regions with over 10 dB of attenuation to the side and behind the instrument due to the mannequin's or musician's body. Directly behind the bodies, increased sound levels occur, as in the balloons of Fig. 5 for $ka = 1$ and $ka = 2$.

At higher frequencies, body effects become even more pronounced. Figure 8 shows the far-field projected directivities for the fifth partial of E4 (1,641 Hz). For the isolated instrument case, three distinct, quasi-axially symmetric interference lobes appear. For the mannequin and played instrument cases, wave effects around the bodies are apparent, although the three lobes remain visible in front of the instrument, with axes tilted according to the clarinet's seated playing orientation.

B. SHADING RESULTS

Figure 9 compares directivity balloons with diffraction effects artificially added in one case through the shading function W_L for the fifth partial of E4 (1,641 Hz), the same partial used for Fig. 8. Theoretical curves as in Fig. 4 determined the attenuation to be $L = 11.2$ dB. Figure 9(a) shows the directivity results from the isolated instrument rotated to conform with the seated orientation of the the blower-mannequin apparatus. Figure 9(b) shows the isolated instrument's shaded directivity and Fig. 9(c) shows the results of the artificially excited instrument with the mannequin. The shading clearly improves the isolated instrument's results, with W_L reducing strong radiation behind the instrument to levels comparable to those produced with the mannequin.

While the shading function W_L effectively mimics the reduced levels behind a musician, it does not include key wave effects such as diffraction lobes and spots. Figure 10 illustrates how the shading function W_s adds these effects for the third partial of E4 (985 Hz) using a spherical radius estimate of $a = 0.2$ m. Without the shading, the isolated instrument's directivity balloon in Fig. 10(a) appears to be roughly omnidirectional, even at this mid frequency. However, the directivity produced by the mannequin-blower apparatus in Fig. 10(c) shows significantly reduced levels and an apparent diffraction spot behind the mannequin. The shaded directivity shown in Fig. 10(b) includes a diffraction spot, reduced levels behind the instrument, and many other similarities.

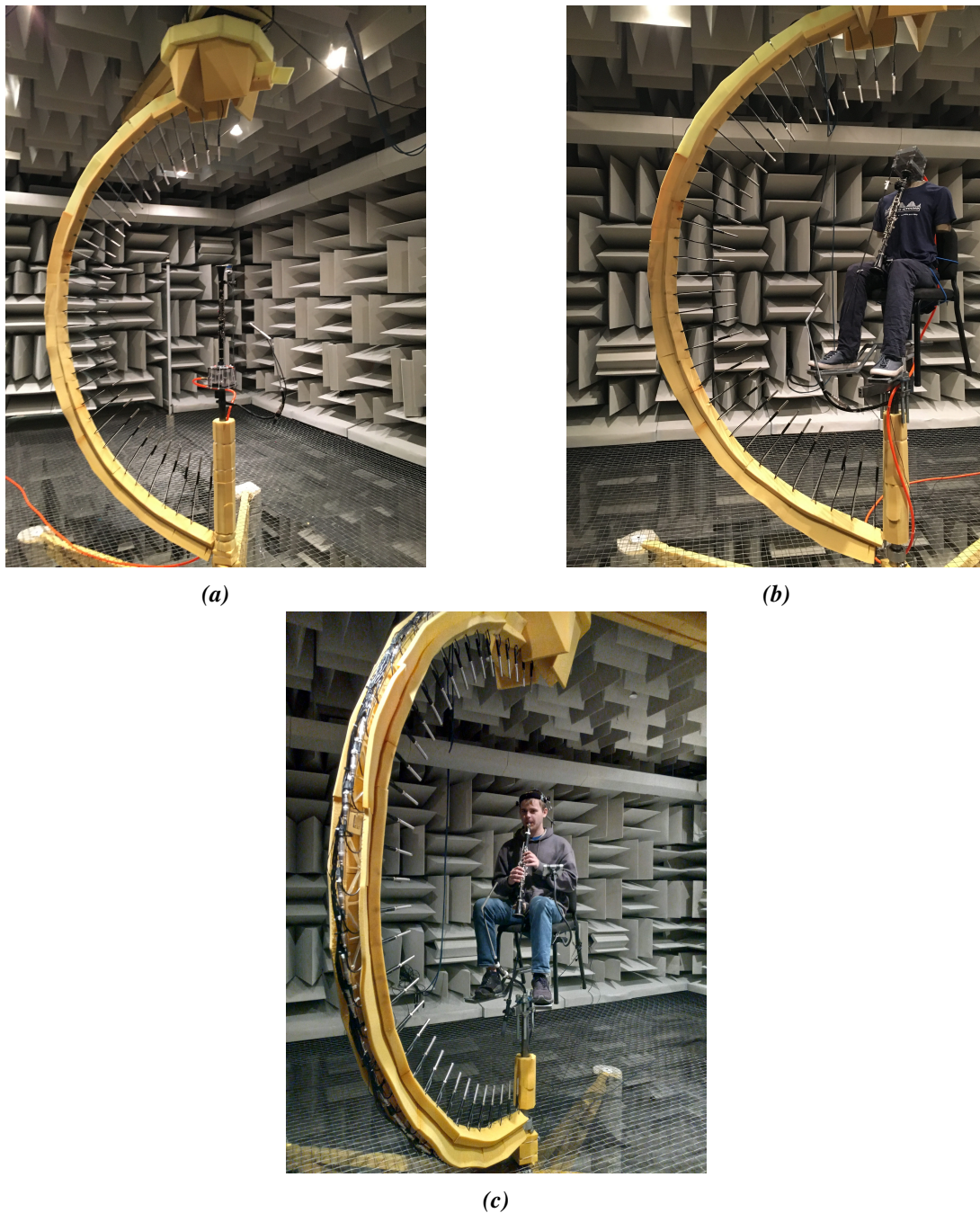


Figure 6: *Three clarinet directivity measurement setups. (a) Isolated clarinet with blowing apparatus, oriented upside down. (b) Clarinet and blowing apparatus attached to a mannequin in playing position, with the blowing apparatus replacing the mannequin head. (c) Naturally played clarinet with a clarinetist.*

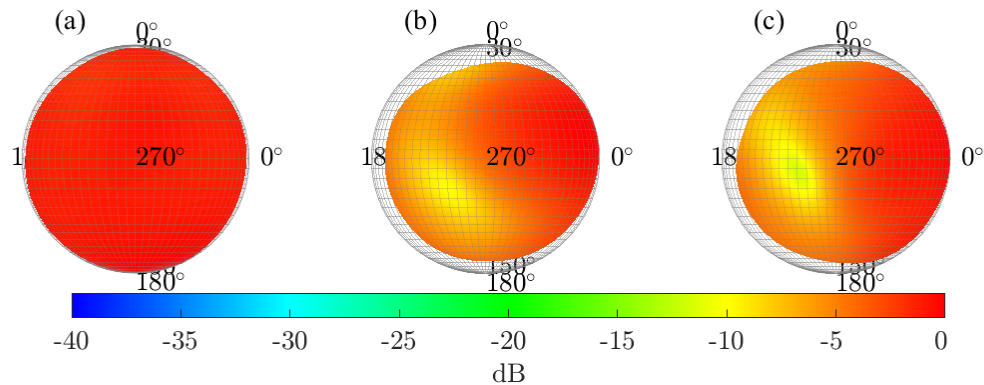


Figure 7: Far-field projected directivity balloons for the clarinet E4 fundamental (328 Hz). (a) Isolated and artificially excited clarinet. (b) Artificially excited clarinet attached to a mannequin. (c) Clarinet played by a musician. All balloons are based on degree $N = 17$ spherical harmonic expansions. The vantage point is from the right side of the instrument. A 180° polar-angle rotation oriented the directivity balloon in (a) so that the bell of the instrument is directed downwards.

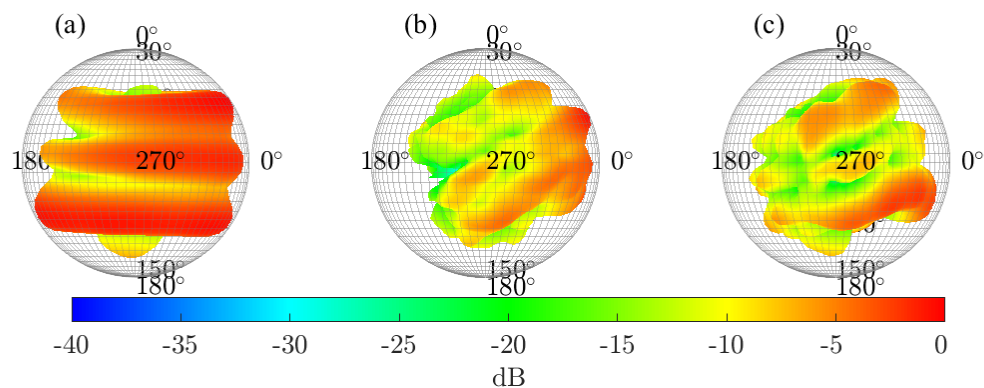


Figure 8: Far-field projected directivity balloons for the fifth partial of E4 (1,641 Hz). (a) Isolated and artificially excited clarinet. (b) Artificially excited clarinet attached to a mannequin. (c) Clarinet played by a musician. The balloons are based on degree $N = 17$ spherical harmonic expansions. The vantage point is from the right side of the instrument. A 180° polar-angle rotation oriented the directivity balloon in (a) so that the bell of the instrument is directed downwards.

6. CONCLUSIONS

The presence of a musician's body plays a critical role in the directivity of a played musical instrument. Incorporating the effects for applications such as room acoustical designs and auralizations is essential. This work suggests that including a mannequin in the measurement setup of an artificially excited instrument improves its directional similarity to a played instrument. If a mannequin is not feasible, a post-processing

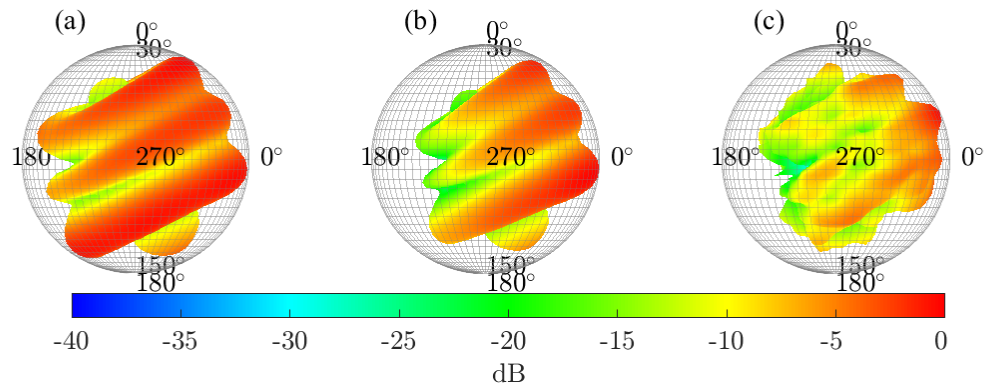


Figure 9: Far-field projected directivity balloons for the fifth partial of E4 (1,641 Hz). (a) Isolated and artificially excited clarinet with seated playing orientation. (b) Isolated and artificially excited clarinet with seated playing orientation and W_L shading applied. (c) Artificially excited clarinet attached to a mannequin. The balloons are based on degree $N = 17$ spherical harmonic expansions. The vantage point is from the right side of the instrument.

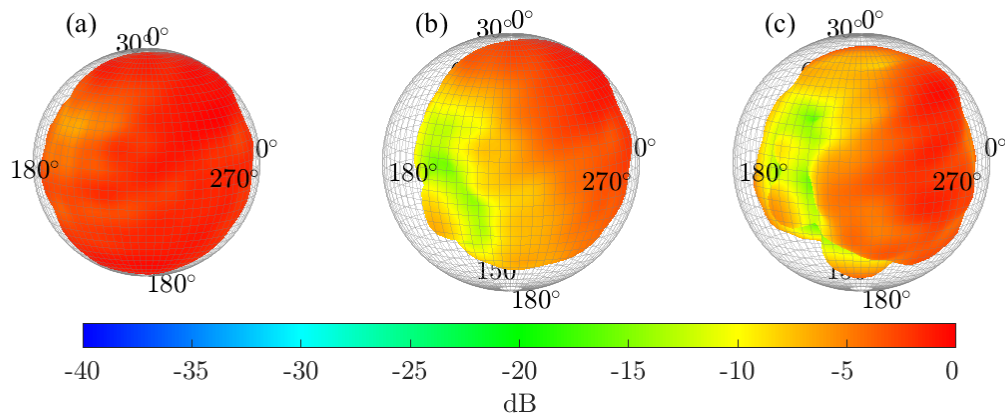


Figure 10: Shading applied to the isolated clarinet directivity for the third partial of E4. Directivity balloons of the (a) isolated instrument rotated to be in the same orientation as the mannequin, (b) shaded isolated instrument (c) instrument and mannequin combination. The balloons are based on degree $N = 17$ spherical harmonic expansions. The vantage point is from the right side of the instrument.

shading function provides angularly dependent attenuation and wave effects as reasonable but less accurate approximations. This work has demonstrated two possible shading functions. Future research may investigate the directional effects of musicians' bodies on other instruments and develop alternative shading functions. Listening tests could also validate whether musician diffraction and absorption are perceptually relevant or not.

ACKNOWLEDGMENTS

The William James and Charlene Fuhrman Strong Family Musical Acoustics Endowed Fellowship Fund funded this research.

REFERENCES

- ¹ J. Meyer and K. Wogram, "Die Richtcharakteristiken des Hornes [The directional characteristics of horns]," *Das Musikinstrument*, **18**(6), pp. I–X, (1969).
- ² T. Grothe and M. Kob, "High resolution 3D radiation measurements on the bassoon," in *Proceedings ISMA*, Detmold, Germany, pp. 139–145, (2019).
- ³ G. Bissinger, E. G. Williams, and N. Valdivia, "Violin f-hole contribution to far-field radiation via patch near-field acoustical holography," *The Journal of the Acoustical Society of America*, **121**(6), pp. 3899–3906, (2007).
- ⁴ G. Weinreich, "Directional tone color," *Journal of the Acoustical Society of America*, **101**(4), pp. 2338–2346, (1997).
- ⁵ J. Meyer, "Die richtcharakteristiken von geigen [the directional characteristics of violins]," *Instrumentenbau-Zeitschrift*, **18**, pp. 275–281, (1964).
- ⁶ L. M. Wang and C. B. Burroughs, "Directivity patterns of acoustic radiation from bowed violins," *CASJ*, **3**(7), pp. 9–17, 1999.
- ⁷ F. Otondo and J. H. Rindel, "The influence of the directivity of musical instruments in a room," *Acta Acustica united with Acustica*, **90**, pp. 1178–1184, (2004).
- ⁸ N. R. Shabtai, G. Behler, M. Vorländer, and S. Weinzierl, "Generation and analysis of an acoustic radiation pattern database for forty-one musical instruments," *The Journal of the Acoustical Society of America*, **141**(2), pp. 1246–1256, (2017).
- ⁹ M. Noistering, F. Zotter, R. Desmonet, and W. Ritsch, "Preserving sound source radiation-characteristics in network-based musical performances," in *Fortschritte der Akustik, DAGA*, Düsseldorf, (2011).
- ¹⁰ C. H. Jeong, J. G. Ih, C. H. Yeon, and C. H. Haan, "Prediction of the acoustic performance of a music hall considering the radiation characteristics of Korean traditional musical sources," *Journal of the Korean Acoustical Society*, **23**(2), pp. 146–161, (2004).
- ¹¹ A. Pérez Carrillo, J. Bonada, J. Pätynen, and V. Välimäki, "Method for measuring violin sound radiation based on bowed glissandi and its application to sound synthesis," *The Journal of the Acoustical Society of America*, **130**(2), pp. 1020–1029, (2011).

-
- ¹² D. Fernandez Comesaña, S. Morales Cervera, T. Takeuchi, and K. Holland, “Measuring musical instruments directivity patterns with scanning techniques,” in *Proceedings of the 19th International Congress on Sound and Vibration*, Vilnius, Lithuania, (2012).
- ¹³ K. J. Bodon, “Development, evaluation, and validation of a high-resolution directivity measurement system for played musical instruments,” Master’s thesis, Brigham Young University, (2016).
- ¹⁴ AES56-2008 (r2014): *AES Standard on Acoustics: Sound Source Modeling: Loudspeaker Polar Radiation Measurements* (Audio Engineering Society, New York, 2015).
- ¹⁵ M. C. Vigeant, L. M. Wang, and J. H. Rindel, “Investigations of orchestra auralizations using the multi-channel multi-source auralization technique,” *Acta Acustica united with Acustica*, **94**, pp. 866–882, (2008).
- ¹⁶ L. Beranek and T. Mellow, *Acoustics: Sound Fields, Transducers and Vibration*. San Diego: Academic Press, (2019).
- ¹⁷ T. W. Leishman, S. D. Bellows, C. M. Pincock, and J. K. Whiting, “High-resolution spherical directivity of live speech from a multiple-capture transfer function method,” *The Journal of the Acoustical Society of America*, **149**(3), pp. 1507–1523, (2021).
- ¹⁸ J. L. Flanagan, “Analog measurements of sound radiation from the mouth,” *Journal of the Acoustical Society of America*, **32**(12), pp. 1613–1620, (1960).
- ¹⁹ F. Bozzoli, M. Viktorovitch, and A. Farina, “Balloons of directivity of real and artificial mouth used in determining speech transmission index,” in *Audio Engineering Society 118*, Barcelona, Spain, (2005).
- ²⁰ J. Meyer, “Die richtcharakteristiken von oboen und fagotten [the directional characteristics of oboes and bassoons.],” *Das Musikinstrument*, **15**, pp. 958–964, (1966).
- ²¹ E. G. Williams, *Fourier Acoustics: Sound Radiation and Nearfield Acoustical Holography*. London: Academic Press, (1999).
- ²² S. D. Bellows and T. W. Leishman, “Acoustic source centering of musical instrument directivities using acoustical holography,” in *Proceedings of Meetings on Acoustics*, **42** (1), (2020).